BJR

■ **BONE BIOLOGY**

N,N-Dimethylformamide inhibits high glucose-induced osteoporosis via attenuating MAPK and NF-κB signalling

Y. D. Liu,
J. F. Liu,
B. Liu

From The First Hospital of Jilin University, Changchun, China

Aims

The role of N,N-dimethylformamide (DMF) in diabetes-induced osteoporosis (DM-OS) progression remains unclear. Here, we aimed to explore the effect of DMF on DM-OS development.

Methods

Diabetic models of mice, RAW 264.7 cells, and bone marrow macrophages (BMMs) were established by streptozotocin stimulation, high glucose treatment, and receptor activator of nuclear factor-κB ligand (RANKL) treatment, respectively. The effects of DMF on DM-OS development in these models were examined by micro-CT analysis, haematoxylin and eosin (H&E) staining, osteoclast differentiation of RAW 264.7 cells and BMMs, H&E and tartrate-resistant acid phosphatase (TRAP) staining, enzyme-linked immunosorbent assay (ELISA) of TRAP5b and c-terminal telopeptides of type 1 (CTX1) analyses, reactive oxygen species (ROS) analysis, quantitative reverse transcription polymerase chain reaction (qRT-PCR), Cell Counting Kit-8 (CCK-8) assay, and Western blot.

Results

The established diabetic mice were more sensitive to ovariectomy (OVX)-induced osteoporosis, and DMF treatment inhibited the sensitivity. OVX-treated diabetic mice exhibited higher TRAP5b and c-terminal telopeptides of type 1 (CTX1) levels, and DMF treatment inhibited the enhancement. DMF reduced RAW 264.7 cell viability. Glucose treatment enhanced the levels of TRAP5b, cathepsin K, Atp6v0d2, and H^+-ATPase, ROS, while DMF reversed this phenotype. The glucose-increased protein levels were inhibited by DMF in cells treated with RANKL. The expression levels of antioxidant enzymes Gclc, Gclm, Ho-1, and Nqo1 were upregulated by DMF. DMF attenuated high glucose-caused osteoclast differentiation by targeting mitogen-activated protein kinase (MAPK) and nuclear factor kappa B (NF-κB) signalling in BMMs.

Conclusion

DMF inhibits high glucose-induced osteoporosis by targeting MAPK and NF-κB signalling.

Article focus

■ This study aimed to explore the effects of N,N-dimethylformamide (DMF) on diabetes-induced osteoporosis (DM-OS) development.

Key messages

■ Streptozotocin-stimulated diabetic mice were more sensitive to ovariectomy (OVX)-induced osteoporosis, and DMF treatment significantly inhibited the osteoporosis.

■ Tartrate-resistant acid phosphatase (TRAP5b) and c-terminal telopeptides of type 1 (CTX1) levels were enhanced in OVX-treated mice, and DMF treatment inhibited the enhancement.

■ DMF treatment reduced RAW 264.7 cell viability.

■ DMF treatment increased the levels of antioxidant enzymes Gclc, Gclm, Ho-1, and Nqo1.

Correspondence should be sent to Bin Liu; email: l_bin@jlu.edu.cn

■ DMF treatment attenuated high glucose-caused osteoclast differentiation by targeting mitogen-activated protein kinase (MAPK) and nuclear factor kappa B (NF-κB) signalling in bone marrow macrophages.

Strengths and limitations
■ These results demonstrate that DMF inhibits high glucose-induced osteoporosis by targeting MAPK and NF-κB signalling.
■ The effects of DMF treatment on DM-OS need to be further confirmed in clinical trials.

Introduction
Osteoporosis is a disorder that reduces bone strength and increases the risk of bone fracture,[1] and the most prevalent basis of bone fractures for older patients.[2] Increasing investigations have revealed that about half of the female and one-quarter of the male population will suffer from osteoporosis-induced bone fractures.[3,4] Because osteoporosis is associated with other diseases, bone loss has become a serious health problem worldwide.[5,6] Diabetes mellitus (DM) is an essential risk factor contributing to the progress of osteoporosis.[7,8] DM-induced osteoporosis (DM-OS) is a general metabolic bone disease that enhances microstructural changes in bone tissues and osteopenia-related fractures, increases friability, and reduces bone strength, a primary complication of DM impacting the skeletal system.[9,10] With the morbidity of DM-OS dramatically increasing, DM-OS has become the principal cause of death and mutilation in diabetes patients,[11] seriously affecting their quality of life and creating a substantial economic burden to their families and society.[12-14] Therefore, there is an urgent need to understand the mechanisms underlying DM-OS.

N,N-dimethylformamide (DMF) is an efficient multipurpose polar catalyst for numerous chemical reactions.[15,16] It can also be used as an efficient ligand in constructing metallic complexes,[17] and as a dehydrating/reducing agent to participate in reactions.[18] More importantly, due to its special structure, DMF is involved in many reactions by functioning as a multi-purpose building block of different units.[19] The biomedical activity of DMF is well-identified in multiple diseases, such as inflammation and cancer.[20,21] However, the effect of DMF on DM-OS remains unknown.

Mitogen-activated protein kinase (MAPK) signalling, an essential pathway in multiple physiological and pathological processes, plays a critical role in modulating osteoporosis, including DM-OS. It has been reported that high glucose suppresses osteogenic differentiation and promotes adipogenicity via cyclic adenosine 3', 5'-monophosphate (cAMP)/protein-kinase A/extracellular signal-regulated kinase signalling in MG-63 cells.[22] Activation of transcription factor-2 and P38 is involved in high extracellular glucose-related osteoblast osmotic response.[23] Exosomes derived from bone marrow mesenchymal stem cells improve osteoporosis by increasing osteoblast proliferation via MAPK pathway.[24] Reduced microRNA-182-5p levels assist alendronate to elevate osteoblast differentiation and proliferation in osteoporosis via Rap1/MAPK signalling pathway.[25] Furthermore, nuclear factor kappa-B (NF-κB) signalling, a critical pathway in multiple cellular processes, contributes to osteoporosis development, and the receptor activator of NF-κB ligand (RANKL) is critically involved in bone healing.[26] MLN64 knockdown inhibits diabetic osteoporosis and represses RANKL-stimulated osteoclastic differentiation by regulating NF-κB signalling in STZ-induced mice.[27] Enhanced expression of the receptor of NF-κB activation decreases runt-related TF2 appearance in the bone from streptozocin-induced diabetic rats.[28] Hydrogen gas prevents ovariectomy-related osteoporosis by repressing NF-κB signalling.[29] *Bifidobacterium longum* NK49 and *Lactobacillus Plantarum* NK3 relieve bacterial vaginosis and osteoporosis by repressing NF-κB-related expression of tumour necrosis factor alpha (TNF-α).[30] Glycyrrhizic acid inhibits postmenopausal osteoporosis and osteoclast differentiation by regulating c-Jun N-terminal kinase (JNK), extracellular signal-related kinase (ERK), and NF-κB signalling.[31] However, the effect of DMF on MAPK and NF-κB signalling in modulating DM-OS remains elusive.

In this study, we aimed to explore the role and the underlying mechanism of DMF in DM-OS progression, and identified a novel inhibitory effect of DMF on DM-OS by modulating MAPK and NF-κB signalling.

Methods
Animals. To investigate the effect of DMF on high glucose-induced osteoporosis, we established a glucose-related osteoporosis mouse model. In brief, 42 female C57BL/6 mice (20 to 22 g, ten weeks old) were randomly divided into control groups (n = 21) and streptozocin treatment groups (n = 21), which were further randomly assigned into sham group (n = 7), ovariectomy (OVX) group (n = 7), and OVX+DMF group (n = 7). Mice in the streptozocin group were intraperitoneally injected with 50 mg/kg streptozotocin (Sigma-Aldrich, USA) for five consecutive days. Blood glucose levels ≥ 16.7 mmol/l were considered as diabetes. Then, the impact of DMF on osteoporosis was analyzed in an OVX-induced osteoporosis mouse model, in which control and diabetic mice were ovariectomized and orally administered DMF (Sigma-Aldrich) daily (30 mg/kg) in 0.6% methocel emulsion (Sigma-Aldrich) for eight weeks. For OVX procedures, after anaesthesia, bilateral incisions were made, and the uterine horn just below the ovary was sutured, followed by ovary extraction. For sham mice, ovaries were raised through the incision site and lowered back. Finally, mice were euthanized, and the femora were obtained. Animal care and experimental procedures in this study were authorized by the Animal Ethics Committee

of our institution. An ARRIVE checklist is included in the Supplementary Material to show that the ARRIVE guidelines were adhered to in this study.

Micro-CT analysis. Bone mineral density (BMD) of the femora was measured by dual-energy x-ray absorptiometry (Hologic Discovery DXA system, Hologic, USA), and a micro-CT system (Skyscan 1176; Bruker-MicroCT, Belgium) was used to analyze the bone microarchitecture and morphology. Femora were scanned at 80 keV and 309 μA with an aluminium plus copper filter, and the images were collected. The BMD, trabecular number (Tb.N), trabecular thickness (Tb.Th), trabecular separation (Tb.Sp), and bone volume per tissue volume (BV/TV) were analyzed using Skyscan CTAn v.1.1.7 software (Bruker-MicroCT).

H&E and TRAP staining analysis of tissue samples. Tissue samples were fixed in 4% paraformaldehyde at 4°C for 24 hours and decalcified in 20% ethylenediaminetetraacetic acid (EDTA) for two weeks. After that, the samples were dehydrated through an ethanol series, embedded in paraffin, and prepared as 4 μm thick sections using a microtome for haematoxylin and eosin (H&E) and tartrate-resistant acid phosphatase (TRAP) staining following the manufacturer's instructions. Histomorphometric analyses of osteoclast numbers were performed using Image-Pro Plus (Media Cybernetics, USA).

Cell culture and treatment. BMMs were obtained from the bone marrow of eight-week-old C57BL/6 mice. The mice were euthanized to collect the tibiae and femora. BMMs were isolated using a syringe and cultured in α-minimum essential medium (MEM) (Thermo Fisher Scientific, USA) with 10% fetal bovine serum and 1% penicillin/streptomycin. Then, the non-adherent cells were cultured with M-CSF (30 ng/ml) at 37°C with 5% CO_2 in a humidified environment for three days until reaching about 90% confluence. RAW 264.7 cells were purchased from American Type Tissue Culture Collection and cultured in Dulbecco's Modified Eagle Medium (DMEM) containing 10% fetal bovine serum, 0.1 mg/ml streptomycin, and 100 units/ml penicillin (all materials from Thermo Fisher Scientific) at 37°C with 5% CO_2.

Bone resorption assay. RAW 264.7 cells and BMMs were plated onto dentine disks (Immunodiagnostic Systems, USA) and treated with 30 ng/ml macrophage colony-stimulating factor (M-CSF) and 50 ng/ml RANKL for five to seven days. After that, cells were completely removed from the dentine disks via abrasion with a cotton tip. Photographs of the resorption pits were obtained under a light microscope at 40× magnification, and the areas were measured using Image-Pro Plus.

F-actin staining. RAW 264.7 cells were fixed with 3.7% formaldehyde and permeabilized with 0.1% Triton X-100. After that, cells were blocked with 1% bovine serum albumin and incubated with 2 U/ml rhodamine phalloidin (Molecular Probes, USA) at room temperature for ten minutes. The experiment was performed in duplicate on four independent occasions in a 24-well plate.

TRAP5b and CTX1 detection. After mice were euthanized, plasma samples were obtained. The expression levels of TRAP5b and CTX1 in plasma samples of mice were measured using enzyme-linked immunosorbent assay (ELISA) kits (TRAP5b and CTX1, Elabscience, China), and the absorbance at 450 nm was measured on a plate reader (BioTek EL 800, BioTek, USA). All procedures were conducted following the manufacturer's instructions.

Osteoclast differentiation and TRAP staining of cells. Approximately 5×10^3 RAW 264.7 cells and 10×10^3 BMMs were plated into 24-well plates and treated with glucose and DMF at indicated doses under the treatment of RANKL (50 ng/ml, five days, R&D Systems, USA). Cells were then fixed in 10% paraformaldehyde for ten minutes and TRAP staining was performed using an acid phosphatase kit (Sigma-Aldrich). The dark red multinucleated cells were considered as TRAP-positive/nucleated cells.

Intracellular reactive oxygen species measurement. In brief, at various times after stimulation with RANKL, confluent cells were washed with α-MEM lacking phenol red and incubated in the dark for five minutes in Krebs-Ringer solution containing 5 μM DCFH-DA. Cells were then observed under a fluorescent microscope and 2,7-dichlorofluorescein (DCF) fluorescence was measured at an excitation of 488 nm and emission of 515 to 540 nm. The fluorescence images were obtained with digital interference contrast, and the mean relative fluorescence intensity for each group of cells was measured using Image-Pro Plus.

Quantitative reverse transcription polymerase chain reaction. Total RNAs were extracted using TRIZOL (Thermo Fisher Scientific). The first-strand complementary DNA (cDNA) was synthesized using Stand cDNA Synthesis Kits (Thermo Fisher Scientific) following the manufacturer's instructions. Quantitative reverse transcription polymerase chain reaction (qRT-PCR) was carried out using SYBR Real-time PCR I kit (Takara, Japan) with glyceraldehyde 3-phosphate dehydrogenase (GAPDH) as the endogenous control. Quantitative determination of RNA levels was conducted by SYBR GreenPremix Ex Taq II Kit (Takara). The experiments were repeated three times. The primers used for qPCR were H+-ATPase forward 5'-ATGGAGCGTCTTGATA AAGCAG-3' and reverse: 5'-CAAGCCGATAGGAACCGTGA-3'; Atp6v0d2 forward 5'-CTGGTTCGAGGATGCAAAGC-3' and reverse 5'-GTTGCCATAGTCCGTGGTCTG -3'; Cathepsin K forward 5'-AGGGAAGCAAGC ACTGGATA-3' and reverse 5'-GCTGGCTGGAATCACATCTT-3'; Gclc forward 5'-CTACCACGCAGTCAAGGACC-3' and reverse 5'-CCTCCATTCAGTAACAACT GGAC-3'; Gclm forward 5'-AGGAGCTTCGGGACTGTATCC-3' and reverse 5'-GGGACATGGTGCATTCCAAAA-3'; Ho-1 forward 5'-AGGTACACATCCAAGCC GAGA-3' and Ho-1 reverse 5'-CATCACCAGCTTAAAGCCTTCT-3'; Nqo1 forward 5'-AGGATGGGAGGTACTCGAATC-3' and Nqo1 reverse 5'-AGGCGTCCTTCCT TATATGCTA-3'; and GAPDH forward 5'-AAGAAGGTGGTGAAGCAGGC-3' and reverse 5'-TCCACCACCCAGTTGCTGTA-3'.
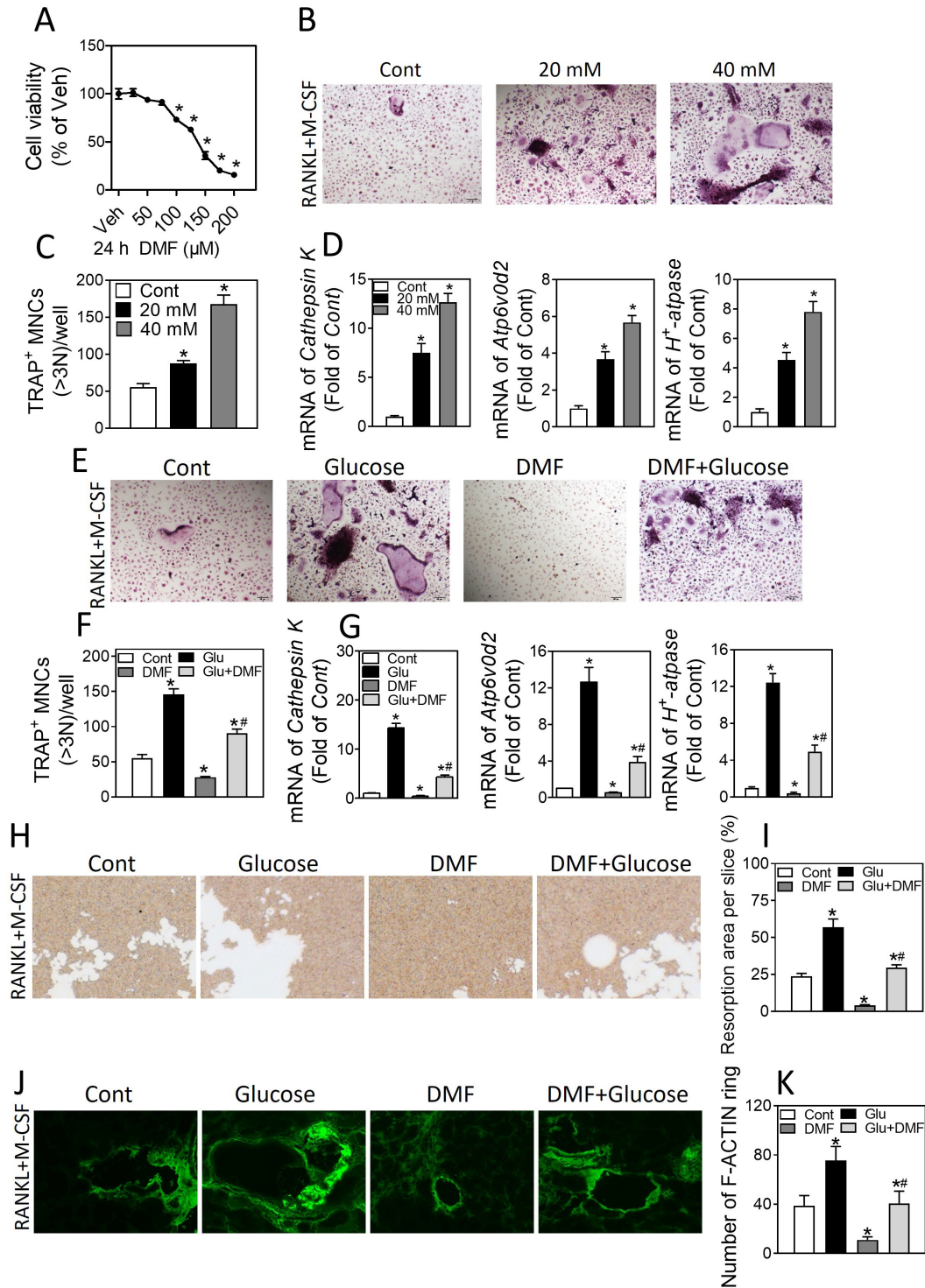
Fig. 1

N,N-dimethylformamide (DMF) inhibits high glucose-enhanced receptor activator of nuclear factor κB ligand (RANKL)-induced osteoclast differentiation in vitro. a) Cell counting kit-8 (CCK-8) measurement of the viability of RAW 264.7 cells treated with DMF at indicated concentrations. The RAW 264.7 cells were treated with glucose at the indicated doses. b) The representative images of tartrate-resistant acid phosphatase (TRAP) staining using an acid phosphatase kit (200×). c) The count of TRAP-positive multinucleated cells containing > three nuclei. d) The expression levels of cathepsin K, Atp6v0d2, and H$^+$-ATPase analyzed by quantitative polymerase chain reaction (qPCR) assays. The RAW 264.7 cells were treated with glucose, DMF, or co-treated with glucose and DMF. e) The representative images of TRAP staining using an acid phosphatase kit (200×). f) The count of TRAP-positive multinucleated cells containing > three nuclei. g) The expression levels of cathepsin K, Atp6v0d2, and H$^+$-ATPase measured by qPCR assays. h) and i) Resorption pits (200×) and j) and k) actin filament (F-ACTIN) were visualized and quantification in cells after seven days of treatment with receptor activator of nuclear factor κB ligand (RANKL) (50 ng/ml) and macrophage colony-stimulating factor (M-CSF) (30 ng/ml) (400×). Data were presented as mean and standard deviation of three independent experiments. *p < 0.05 versus control, #p < 0.05 versus glucose treatment (two-way analysis of variance). mRNA, messenger RNA.
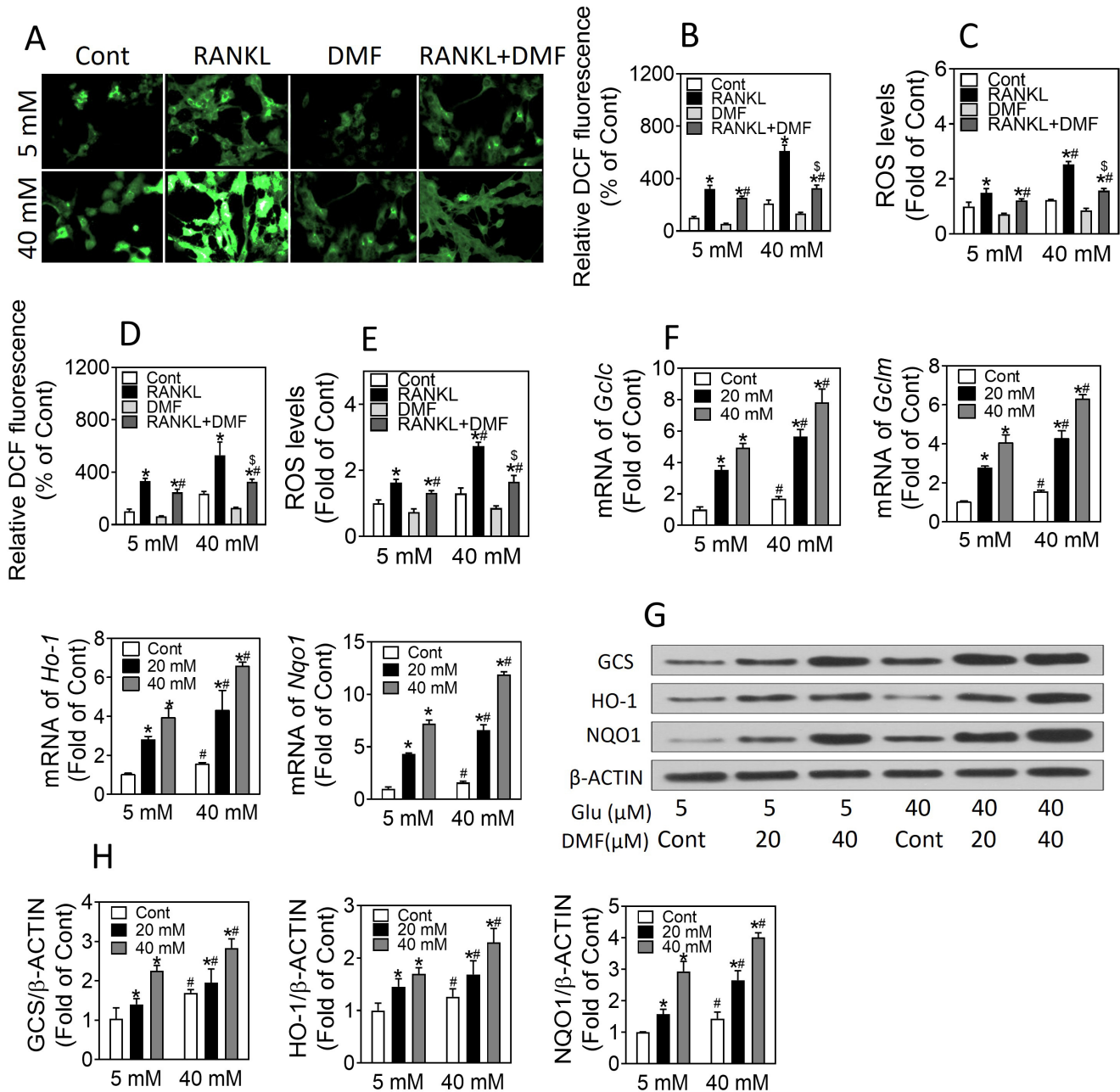
Fig. 2

N,N-dimethylformamide (DMF) inhibits high glucose-induced reactive oxygen species (ROS) accumulation. a) The glucose-treated (5 mM or 40 mM) bone marrow macrophages (BMMs) were preloaded with dichloro-dihydro-fluorescein diacetate (DCFH-DA) and treated with 50 ng/ml receptor activator of nuclear factor κB ligand (RANKL), 20 μM DMF, or their combination (×400). The ROS levels were assessed by flow cytometry analysis. The representative microscopic fields are shown: b) the relative intensity of DCF fluorescence in BMMs and d) RAW 264.7 cells. The c) glucose-treated (5 mM or 40 mM) BMMs and e) RAW 264.7 cells were treated with 50 ng/ml RANKL, 20 μM DMF, or a combination of the two. ROS levels were assessed by flow cytometry analysis. The glucose-treated (5 mM or 40 mM) RAW 264.7 cells were treated with DMF at the indicated dose. f) The messenger RNA (mRNA) levels of *Gclc*, *Gclm*, *Ho-1*, and *Nqo1* were examined by quantitative polymerase chain reaction. g) The protein levels of GCS, HO-1, and NQO1 were tested by Western blot. h) Western blot results were quantified by ImageJ software (National Institutes of Health, USA). Data were presented as mean and standard deviation of three independent experiments. *p < 0.05 versus control of the same glucose concentration group, #p < 0.05 versus 5 mM glucose with the same DMF and/or RANKL treatment. $p < 0.05 versus the same glucose concentration plus RANKL treatment (two-way analysis of variance).

CCK-8 assays. Cell viability was analyzed by cell counting kit-8 (CCK-8) assays. Approximately 5×10^3 cells were seeded into 96 wells. After having been cultured for 12 hours, cells were treated with DMF at different concentrations for 24 hours. The cells were then incubated with CCK-8 solution (KeyGEN Biotech, China) and cultured for another two hours at 37°C. Absorbance at 450 nm was measured using a microplate reader (BioTek EL 800).

Analysis of ROS levels. The intracellular ROS levels were measured by flow cytometry analysis. The glucose-treated

(5 mM or 40 mM) RAW 264.7 cells were treated with RANKL (50 ng/ml), DMF (20 µM), or co-treated with RANKL and DMF for 60 minutes. After being washed with PBS three times, cells were incubated with DCF at 37°C for 60 minutes and re-suspended in flow cytometry (FACS) buffer. The fluorescence was detected using a Flow cytometry system (BD Biosciences, USA) with an excitation wavelength of 488 nm and emission wavelength of 525 nm. The results were analyzed using FlowJoO software (TreeStar, USA).

Western blot analysis. Total proteins were extracted from the cells with radioimmunoprecipitation assay (RIPA) buffer (Cell Signaling Technology (CST), USA). Protein concentrations were measured using the BCA Protein Quantification Kit (Abbkine, USA). The same amounts of proteins were separated by sodium dodecyl sulphate-polyacrylamide gel electrophoresis (SDS-PAGE) (12% polyacrylamide gels) and transferred onto polyvinylidene difluoride (PVDF) membranes (MilliporeSigma, USA). The membranes were blocked with 5% milk and incubated overnight at 4°C with primary antibodies from Santa-Cruz Biotechnology (USA) against β-actin (sc-1616), GCS (sc-390811), HO-1 (sc-390991), and NQO1 (sc-32793) and primary antibodies from CST against p-NF-κB (3033), NF-κB (3032), p-IκBα (8219), IκBα (9242), p-ERK (4370), ERK (4695), p-JNK (9251), JNK (9252), p-P38 (9215), P38 (9212), TRAF6 (8028), and RANK (4845). After that, the membranes were further incubated with horseradish peroxidase (HRP)-linked anti-rabbit immunoglobulin G (IgG) secondary antibody (1:3,000) in tris-buffered saline (TBST) for one hour. After being washed with TBST three times, the membranes were developed with enhanced chemiluminescence using enhanced chemiluminescence (ECL) reagents. The bands were visualized by the LI-COR Odyssey FC infrared imaging system (LI-COR, USA).

Statistical analysis. Data were presented as mean and standard deviation (SD), and analyzed using GraphPad Prism 7 (USA). The independent-samples *t*-test was used for comparison between two groups, and one-way or two-way analysis of variance (ANOVA) was used for comparison among multiple groups with Bonferroni post hoc tests. Differences with $p < 0.05$ were considered statistically significant.

Results

DMF attenuates high glucose-induced susceptibility to osteoporosis in vivo. To assess the effect of DMF on high glucose-induced osteoporosis, a glucose-related osteoporosis mouse model was established and treated with DMF. As expected, the blood glucose levels were over 16.7 mmol/l in the mice treated with streptozotocin, indicating that the diabetic mouse model was successfully established ($p = 0.038$, two-way ANOVA) (Supplementary Figure aa). The dual-energy X-ray absorptiometry and micro-CT analyses showed that streptozotocin-stimulated diabetic mice were more sensitive to OVX-induced osteoporosis, and DMF treatment significantly inhibited

osteoporosis in the system (Supplementary Figures ab and ac) and reversed the levels of Tb.N, Tb.Th, Tb.Sp, and BV/TV ($p = 0.015$, two-way ANOVA) (Supplementary Figure ad). H&E and TRAP staining analyses showed that DMF effectively inhibited streptozotocin-enhanced osteoclast differentiation (Supplementary Figure ae to ag). In addition, the expression levels of bone metabolism biomarkers TRAP5b and CTX1 were enhanced in OVX-treated mice, and DMF inhibited these enhancements ($p = 0.026$, two-way ANOVA) (Supplementary Figure ah). These data suggest that DMF relieves high glucose-induced susceptibility to osteoporosis in vivo.

DMF suppresses high glucose-induced osteoclast differentiation in vitro. The role of DMF in high glucose-related osteoporosis was then explored in vitro. RAW 264.7 cells were treated with different concentrations of DMF. CCK-8 assays revealed that DMF treatment reduced RAW 264.7 cell viability in a dose-dependent manner with 80% survival at 75 µM ($p = 0.016$, two-way ANOVA) (Figure 1a), which was therefore selected as the dosage for subsequent experiments. As expected, glucose significantly increased TRAP accumulation in a dose-dependent manner, as demonstrated by the representative TRAP staining images (Figure 1b) and the increased count of TRAP-positive multinucleated cells containing > three nuclei from 50 in the control group to 150 in the DMF-treated group ($p = 0.024$, two-way ANOVA) (Figure 1c). Furthermore, glucose treatment upregulated the expression of Cathepsin K, Atp6v0d2, and H$^+$-ATPase in a dose-dependent manner ($p = 0.027$, two-way ANOVA) (Figure 1d), indicating that glucose exposure induces osteoclast differentiation. Moreover, DMF suppressed the levels of TRAP promoted by glucose treatment in the RAW 264.7 cells as revealed by the representative images of TRAP staining (Figure 1e) and the count of TRAP-positive multinucleated cells containing > three nuclei ($p = 0.011$, two-way ANOVA) (Figure 1f). Meanwhile, the increased expression levels of Cathepsin K, Atp6v0d2, and H$^+$-ATPase by glucose were reversed by DMF treatment ($p = 0.015$, two-way ANOVA) (Figure 1g). Actin filament (F-ACTIN) rings and bone pit analysis showed that DMF treatment also reversed the enhancing effect induced by high glucose levels (Figure 1k), suggesting that DMF inhibited osteoclast differentiation induced by high glucose in vitro.

DMF inhibits high glucose-induced reactive oxygen species accumulation. As high glucose can increase reactive oxygen species (ROS) accumulation, the impact of DMF on ROS levels in BMMs and RAW 264.7 cells treated with RANKL was further investigated. The results showed that DMF inhibited glucose-increased ROS levels under RANKL treatment in these cells ($p < 0.05$) (Figure 2e). Moreover, the expression levels of antioxidant enzymes Gclc, Gclm, Ho-1, and Nqo1 were elevated around five-fold by DMF treatment ($p = 0.027$, two-way ANOVA) (Figure 2f). Furthermore, DMF increased the expression levels of GCS, HO-1, and NQO1 in a dose-dependent manner ($p = 0.031$, two-way ANOVA) (Figure 2h). Together these data
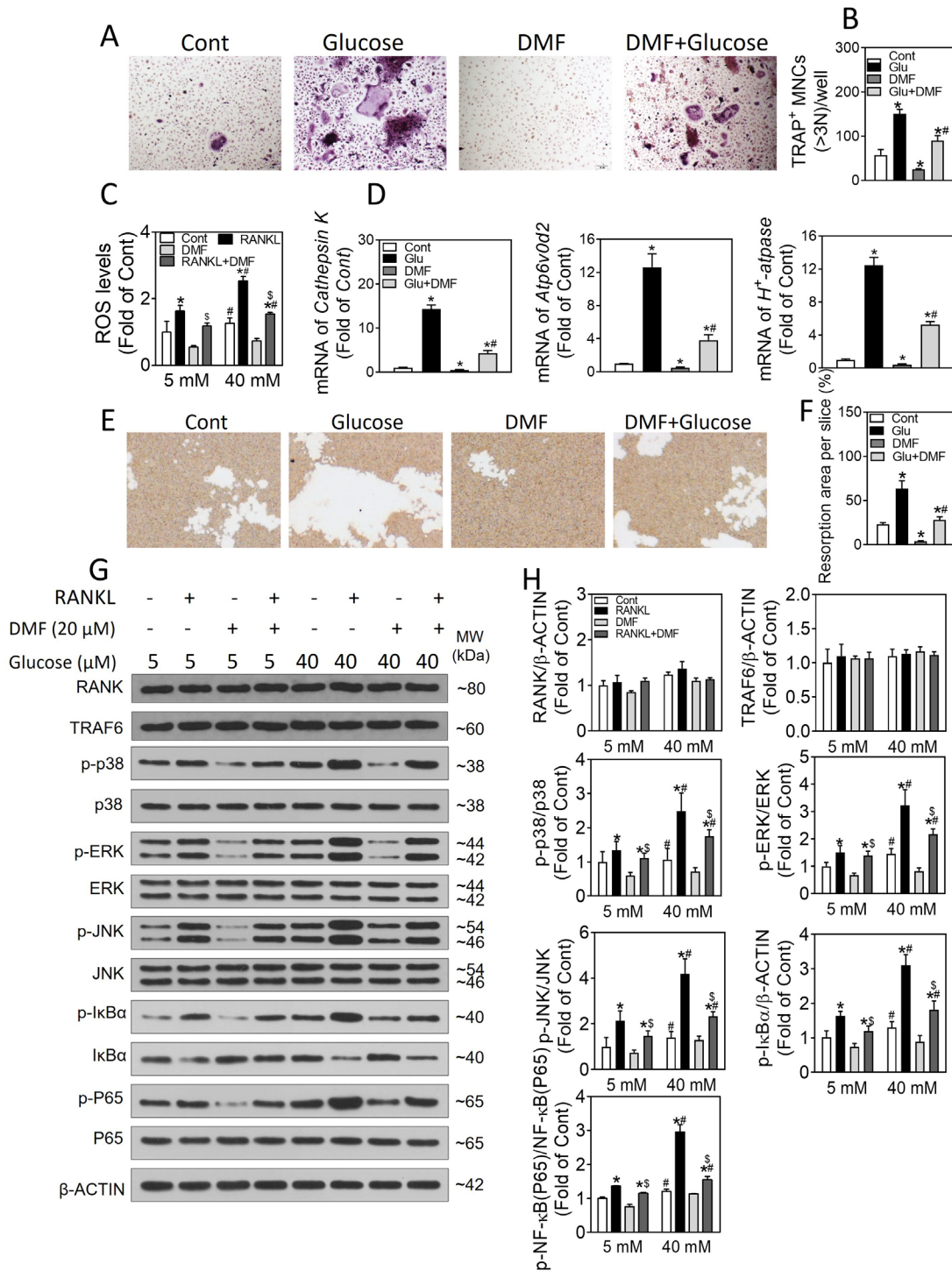
Fig. 3

N,N-Dimethylformamide (DMF) inhibits high glucose-caused osteoclast differentiation by targeting mitogen-activated protein kinase (MAPK) signalling and nuclear factor kappa B (NF-κB) signalling in bone marrow macrophages (BMMs). The glucose-treated BMMs were treated with receptor activator nuclear factor κB ligand (RANKL), DMF, or their combination for 30 minutes. a) Reactive oxygen species (ROS) levels were assessed by flow cytometry analysis (×200). b) Tartrate-resistant acid phosphatase (TRAP) staining was performed using an acid phosphatase kit, and the representative images of TRAP staining were shown. c) The count of TRAP-positive multinucleated cells containing > three nuclei was presented. d) The expression levels of cathepsin K, Atp6v0d2, and H^+-ATPase were analyzed by quantitative polymerase chain reaction (qPCR) assays. e) and f) Following seven days of treatment with RANKL (50 ng/ml) and macrophage colony-stimulating factor (M-CSF) (30 ng/ml), cells were removed from the dentine discs, and resorption pits were visualized. g) The levels of RANK, TRAF6, P38, extracellular signal-related kinase (ERK), JNK, NF-κB (p65), IκBα, β-ACTIN and phosphorylated P38, ERK, JNK, NF-κB (p65), and IκBα were measured by Western blot. h) The results of Western blot analysis were quantified by ImageJ software (National Institutes of Health, USA). Data were presented as mean and standard deviation of three independent experiments. *$p < 0.05$ versus control of the same glucose concentration, #$p < 0.05$ versus 5 mM glucose with the same DMF and/or RANKL treatment, $$p < 0.05$ versus the same glucose concentration plus RANKL treatment (two-way analysis of variance). mRNA, messenger RNA.

suggest that DMF inhibited high glucose-induced ROS accumulation.

DMF inhibits high glucose-activated MAPK and NF-κB signalling. Next, the mechanism of DMF-induced protective effect against high glucose-related osteoporosis was investigated. Since MAPK pathway and NF-κB pathway play crucial roles in osteoclastogenesis and osteoclast differentiation, we speculated that DMF exerted its function by targeting MAPK and NF-κB signalling pathways. Western blot analysis revealed that DMF reduced high glucose-induced phosphorylation of P38, ERK, and JNK (p = 0.036, two-way ANOVA) as well as high glucose-induced phosphorylation of NF-κB (p65) and IκBα (p = 0.193, two-way ANOVA) (Supplementary Figure ba and bb). These results indicated that DMF inhibited high glucose-activated MAPK signalling and NF-κB signalling pathways.

DMF inhibits high glucose-caused osteoclast differentiation by targeting MAPK signalling and NF-κB signalling in BMMs. To further validate the inhibitory effect of DMF on high glucose-caused osteoclast differentiation, bone marrow macrophages (BMMs) were treated with DMF. The results showed that DMF reduced high glucose-promoted ROS levels in BMMs with RANKL treatment (p = 0.023, one-way ANOVA) (Figure 3a). As expected, DMF inhibited high dose glucose-enhanced accumulation of TRAP in BMMs, as demonstrated by the representative images of TRAP staining (Figure 3b) and the count of TRAP-positive multinucleated cells containing > three nuclei (p = 0.034, two-way ANOVA) (Figure 3c). Moreover, DMF treatment reversed high-glucose enhanced expression levels of Cathepsin K, Atp6v0d2, and H+-ATPase (p = 0.018, one-way ANOVA) (Figure 3d), suggesting that DMF inhibited high glucose-induced osteoclast differentiation. Furthermore, DMF treatment reversed the enhancing effect of high glucose levels on bone pits (Figure 3f) and attenuated high glucose-activated phosphorylation of P38, ERK, JNK, NF-κB (p65), and IκBα (p = 0.029, two-way ANOVA) (Figure 3h), indicating that DMF relieved high glucose-caused osteoclast differentiation via targeting MAPK and NF-κB signalling pathways in BMMs.

Discussion

DM-OS is a severe disorder that affects increasing numbers of patients and is associated with multiple complications.[32,33] As a multipurpose reagent, DMF has displayed potential biomedical activities in multiple diseases. For example, DMF has dual impacts on apoptosis and proliferation of breast cancer cells, depending on its concentration.[34] It induces a characteristic change of cells and suppresses tumorigenesis in human colon carcinoma cells.[35] DMF also inhibits cisplatin-related kidney injury by stimulating the Nrf2 pathway and repressing the NF-κB pathway.[36] DMF affects Kdo glycosylation by stereoselective synthesis for α-Kdo glycosides,[37] and regulates standard conversion potentials for oxygen and carbon dioxide couples.[38] In this study, we found that DMF inhibits high glucose-induced susceptibility to osteoporosis in vivo

and suppresses high glucose-induced osteoclast differentiation in vitro. These data demonstrated an unreported function of DMF in DM-related osteoporosis, providing new insights into the biomedical activity of DMF.

Previous studies have indicated that overdose of DMF causes hepatic cytotoxicity,[39,40] which leads to the consideration of choosing the appropriate dose for disease treatment. Moreover, DMF is known to elicit certain alcohol intolerance reactions.[41] Hence, appropriate application strategies should be designed, and patients with histories of alcohol abuse should be particularly counselled. Notably, our data showed no obvious toxicity of DMF to mice, possibly due to the low dose we adopted in this work.

ROS are required for cell signal transduction and other physiological functions, and are involved in modulating osteoporosis, including DM-related osteoporosis.[42] Activation of ROS/MAPKs/NF-κB/NLRP3 and efferocytosis inhibition have been observed in osteoclast-related diabetes osteoporosis.[43] Loureirin B represses RANKL-stimulated ovariectomized osteoporosis and osteoclast genesis by inhibiting the actions of NFATc1 and ROS.[44] Pseurotin A represses osteoclast genesis and inhibits ovariectomized-produced bone loss via ROS.[45] Vitamin B5 restrains RANKL-related osteoclast genesis and ovariectomy-induced osteoporosis by modulating ROS production.[46] Sesamin preserves osteonecrosis-related femoral head by repressing ROS-induced osteoblast apoptosis in rat models.[47] Angelica polysaccharide promotes proliferation and osteoblast differentiation of mesenchymal stem cells by regulating long non-coding RNA H19.[48] Low concentration of dexamethasone influences osteoblast viability by provoking autophagy via mediating ROS.[49] Irbesartan inhibits unconventional glycation end product-regulated damage in DM-OS by mediating ROS.[50] In our work, we found that DMF suppresses glucose-stimulated ROS production and simultaneously elevates the levels of antioxidant enzymes including Gclc, Gclm, Ho-1, and Nqo1 in a dose-dependent manner. These data reveal that DMF inhibits high glucose-induced ROS accumulation and demonstrates a novel correlation of DMF with ROS in modulating DM-OS.

As the fundamental cellular signalling pathways, MAPK signalling and NF-κB signalling pathways are involved in the progression of osteoporosis, including DM-OS, and serve as potential targets for anti-osteoporosis treatment. It has been reported that quercitrin inhibits osteoporosis by controlling MAPK signalling in ovariectomized rats.[51] Timosaponin AIII inhibits inflammation injury in Alloxan-stimulated diabetic osteoporosis in zebrafish AGEs-produced osteoblasts by regulating MAPK signalling.[52] Taurine stimulates BMP-2/Wnt3a-related mineralization and osteoblast differentiation by regulating MAPK signalling.[53] Bergapten exercises inhibitory influences on DM-OS by modulating NF-κB and JNK/MAPK signalling in vivo.[54] Meanwhile, a previous study has identified that proanthocyanidins repress the formation and function of osteoclasts by restraining JNK and NF-κB signalling under

osteoporosis treatment.[55] Ferulic acid inhibits osteoporosis by stimulating SIRT1 and NF-κB in glucocorticoid-related osteoporosis neonatal rats.[56] Icariin abolishes osteoclast formation by modulating RANKL-induced TRAF6/NF-κB/ERK signalling in Raw 264.7 cells.[57] Stattic represses RANKL-stimulated osteoclast genesis by inhibiting STAT3 and NF-κB activation.[58] Inhibiting NF-κB signalling pathway by anthracycline glycoside aloin plays a part in the osteoclast genesis.[59] Tubeimoside I suppresses RANKL-stimulated NF-κB signalling, osteoclast formation, and diabetes-related bone loss in rats.[60] Apolipoprotein E presents a critical function in preserving bone mass by increasing osteoblast differentiation via ERK1/2 pathway and by repressing osteoclast differentiation via NF-κB signalling.[61] Coincidently, one previous study has demonstrated the function of DMF in oxidation and its correlation with NF-κB signalling.[36] Therefore, we examined whether NF-κB signalling is involved in DMF-alleviated DM-OS, and obtained the expected results that DMF administration decreases phosphorylation of IκBα and its downstream NF-κB, together with inactivation of p38, ERK, and JNK signalling.

In conclusion, we found that DMF inhibits high glucose-induced osteoporosis by targeting MAPK and NF-κB signalling and uncovered a novel inhibitory effect of DMF on DM-OS. The study indicates that DMF might serve as a potential candidate for DM-OS treatment.

Supplementary material

ë An ARRIVE checklist is included to show that the ARRIVE guidelines were adhered to in this study, as well as supplementary figures expanding on the study results.

References

1. **Miller PD**. Management of severe osteoporosis. *Expert Opin Pharmacother*. 2016;17(4):473–488.
2. **Coughlan T**, **Dockery F**. Osteoporosis and fracture risk in older people. *Clin Med*. 2014;14(2):187–191.
3. **Jemtland R**, **Holden M**, **Reppe S**, **et al**. Molecular disease map of bone characterizing the postmenopausal osteoporosis phenotype. *J Bone Miner Res*. 2011;26(8):1793–1801.
4. **Chao TH**, **Yu HN**, **Huang CC**, **Liu WS**, **Tsai YW**, **Wu WT**. Association of interleukin-1 beta (-511C/T) polymorphisms with osteoporosis in postmenopausal women. *Ann Saudi Med*. 2010;30(6):437–441.
5. **Varenna M**, **Manara M**, **Galli L**, **Binelli L**, **Zucchi F**, **Sinigaglia L**. The association between osteoporosis and hypertension: the role of a low dairy intake. *Calcif Tissue Int*. 2013;93(1):86–92.
6. **Armas LAG**, **Recker RR**. Pathophysiology of osteoporosis: new mechanistic insights. *Endocrinol Metab Clin North Am*. 2012;41(3):475–486.
7. **Hofbauer LC**, **Brueck CC**, **Singh SK**, **Dobnig H**. Osteoporosis in patients with diabetes mellitus. *J Bone Miner Res*. 2007;22(9):1317–1328.
8. **Kurra S**, **Fink DA**, **Siris ES**. Osteoporosis-associated fracture and diabetes. *Endocrinol Metab Clin North Am*. 2014;43(1):233–243.
9. **Paschou SA**, **Dede AD**, **Anagnostis PG**, **Vryonidou A**, **Morganstein D**, **Goulis DG**. Type 2 diabetes and osteoporosis: a guide to optimal management. *J Clin Endocrinol Metab*. 2017;102(10):3621–3634.
10. **Mohsin S**, **Baniyas MM**, **AlDarmaki RS**, **Tekes K**, **Kalász H**, **Adeghate EA**. An update on therapies for the treatment of diabetes-induced osteoporosis. *Expert Opin Biol Ther*. 2019;19(9):937–948.
11. **Giovos G**, **Yavropoulou MP**, **Yovos JG**. The role of cellular senescence in diabetes mellitus and osteoporosis: molecular pathways and potential interventions. *Hormones*. 2019;18(4):339–351.
12. **Raška I Jr**, **Rašková M**, **Zikán V**, **Škrha J**. Prevalence and risk factors of osteoporosis in postmenopausal women with type 2 diabetes mellitus. *Cent Eur J Public Health*. 2017;25(1):3–10.
13. **Li S**, **Mao Y**, **Zhou F**, **Yang H**, **Shi Q**, **Meng B**. Gut microbiome and osteoporosis: a review. *Bone Joint Res*. 2020;9(8):524–530.
14. **Zheng W**, **Liu C**, **Lei M**, **et al**. Evaluation of common variants in the CNR2 gene and its interaction with abdominal obesity for osteoporosis susceptibility in Chinese postmenopausal females. *Bone Joint Res*. 2019;8(11):544–549.
15. **Le Bras J**, **Muzart J**. Recent uses of N,N-dimethylformamide and N,N-dimethylacetamide as reagents. *Molecules*. 2018;23(8):E1939.
16. **Ding S**, **Jiao N**. N,N-dimethylformamide: a multipurpose building block. *Angew Chem Int Ed Engl*. 2012;51(37):9226–9237.
17. **Lu S-R**, **Lai Y-H**, **Chen J-H**, **Liu C-Y**, **Mong K-K**. Dimethylformamide: an unusual glycosylation modulator. *Angew Chem Int Ed Engl*. 2011;50(32):7315–7320.
18. **Kennedy GL**. Toxicology of dimethyl and monomethyl derivatives of acetamide and formamide: a second update. *Crit Rev Toxicol*. 2012;42(10):793–826.
19. **Li MJ**, **Zeng T**. The deleterious effects of N,N-dimethylformamide on liver: a mini-review. *Chem Biol Interact*. 2019;298:129–136.
20. **Gumilar F**, **Agotegaray M**, **Bras C**, **Gandini NA**, **Minetti A**, **Quinzani O**. Antinociceptive activity and toxicity evaluation of Cu(II)-fenoprofenate complexes in mice. *Eur J Pharmacol*. 2012;675(1–3):32–39.
21. **Allison M**, **Wilson D**, **Pask CM**, **McGowan PC**, **Lord RM**. β-Diketonate versus β-Ketoiminate: the importance of a ferrocenyl moiety in improving the anticancer potency. *Chembiochem*. 2020;21(14):1988–1996.
22. **Wang W**, **Zhang X**, **Zheng J**, **Yang J**. High glucose stimulates adipogenic and inhibits osteogenic differentiation in MG-63 cells through cAMP/protein kinase A/extracellular signal-regulated kinase pathway. *Mol Cell Biochem*. 2010;338(1–2):115–122.
23. **Zayzafoon M**, **Botolin S**, **McCabe LR**. P38 and activating transcription factor-2 involvement in osteoblast osmotic response to elevated extracellular glucose. *J Biol Chem*. 2002;277(40):37212–37218.
24. **Zhao P**, **Xiao L**, **Peng J**, **Qian YQ**, **Huang CC**. Exosomes derived from bone marrow mesenchymal stem cells improve osteoporosis through promoting osteoblast proliferation via MAPK pathway. *Eur Rev Med Pharmacol Sci*. 2018;22(12):3962–3970.
25. **Pan B-L**, **Tong Z-W**, **Li S-D**, **et al**. Decreased microRNA-182-5p helps alendronate promote osteoblast proliferation and differentiation in osteoporosis via the Rap1/MAPK pathway. *Biosci Rep*. 2018;38(6):BSR20180696.
26. **Starlinger J**, **Kaiser G**, **Thomas A**, **Sarahrudi K**. The impact of nonosteogenic factors on the expression of osteoprotegerin and RANKL during human fracture healing. *Bone Joint Res*. 2019;8(7):349–356.
27. **Lei C**, **Xueming H**, **Ruihang D**. MLN64 deletion suppresses RANKL-induced osteoclastic differentiation and attenuates diabetic osteoporosis in streptozotocin (STZ)-induced mice. *Biochem Biophys Res Commun*. 2018;505(4):1228–1235.
28. **Hie M**, **Tsukamoto I**. Increased expression of the receptor for activation of NF-kappaB and decreased runt-related transcription factor 2 expression in bone of rats with streptozotocin-induced diabetes. *Int J Mol Med*. 2010;26(4):611–618.
29. **Wu G**, **Pan L**, **Sun J**, **Chen G**, **Wang S**. Hydrogen gas protects against ovariectomy-induced osteoporosis by inhibiting NF-κB activation. *Menopause*. 2019;26(7):785–792.
30. **Kim DE**, **Kim JK**, **Han SK**, **Jang SE**, **Han MJ**, **Kim DH**. Lactobacillus plantarum NK3 and bifidobacterium longum NK49 alleviate bacterial vaginosis and osteoporosis in mice by suppressing NF-κB-linked TNF-α expression. *J Med Food*. 2019;22(10):1022–1031.
31. **Yin Z**, **Zhu W**, **Wu Q**, **et al**. Glycyrrhizic acid suppresses osteoclast differentiation and postmenopausal osteoporosis by modulating the NF-κB, ERK, and JNK signaling pathways. *Eur J Pharmacol*. 2019;859:172550.
32. **Sealand R**, **Razavi C**, **Adler RA**. Diabetes mellitus and osteoporosis. *Curr Diab Rep*. 2013;13(3):411–418.
33. **de Quadros VP**, **Tobar N**, **Viana LR**, **dos Santos RW**, **Kiyataka PHM**, **Gomes-Marcondes MCC**. The 17β-oestradiol treatment minimizes the adverse effects of protein restriction on bone parameters in ovariectomized Wistar rats. *Bone Joint Res*. 2019;8(12):573–581.
34. **Zhang J**, **Zhou D**, **Zhang L**, **et al**. Dual effects of N,N-dimethylformamide on cell proliferation and apoptosis in breast cancer. *Dose Response*. 2017;15(4):1559325817744450.
35. **Dexter DL**, **Barbosa JA**, **Calabresi P**. N,N-dimethylformamide-induced alteration of cell culture characteristics and loss of tumorigenicity in cultured human colon carcinoma cells. *Cancer Res*. 1979;39(3):1020–1025.

36. **Zhao K**, **Wen LB**. DMF attenuates cisplatin-induced kidney injury via activating Nrf2 signaling pathway and inhibiting NF-kB signaling pathway. *Eur Rev Med Pharmacol Sci*. 2018;22(24):8924–8931.

37. **Lou Q**, **Hua Q**, **Zhang L**, **Yang Y**. Dimethylformamide-modulated kdo glycosylation for stereoselective synthesis of α-kdo glycosides. *Org Lett*. 2020;22(3):981–985.

38. **Pegis ML**, **Roberts JAS**, **Wasylenko DJ**, **Mader EA**, **Appel AM**, **Mayer JM**. Correction to standard reduction potentials for oxygen and carbon dioxide couples in acetonitrile and N,N-dimethylformamide. *Inorg Chem*. 2020;59(12):8638.

39. **Li S**, **Wang C**. Study on the potential way of hepatic cytotoxicity of N,N-dimethylformamide. *J Biochem Mol Toxicol*. 2018;32(9):e22190.

40. **Kim TH**, **Kim YW**, **Shin SM**, **Kim CW**, **Yu IJ**, **Kim SG**. Synergistic hepatotoxicity of N,N-dimethylformamide with carbon tetrachloride in association with endoplasmic reticulum stress. *Chem Biol Interact*. 2010;184(3):492–501.

41. **Kilo S**, **Göen T**, **Drexler H**. Cross-sectional study on N,N-dimethylformamide (DMF); effects on liver and alcohol intolerance. *Int Arch Occup Environ Health*. 2016;89(8):1309–1320.

42. **Agidigbi TS**, **Kim C**. Reactive Oxygen Species in Osteoclast Differentiation and Possible Pharmaceutical Targets of ROS-Mediated Osteoclast Diseases. *Int J Mol Sci*. 2019;20(14):3576.

43. **An Y**, **Zhang H**, **Wang C**, **et al**. Activation of ROS/MAPKs/NF-κB/NLRP3 and inhibition of efferocytosis in osteoclast-mediated diabetic osteoporosis. *FASEB J*. 2019;33(11):12515–12527.

44. **Liu Y**, **Wang C**, **Wang G**, **et al**. Loureirin B suppresses RANKL-induced osteoclastogenesis and ovariectomized osteoporosis via attenuating NFATc1 and ROS activities. *Theranostics*. 2019;9(16):4648–4662.

45. **Chen K**, **Qiu P**, **Yuan Y**, **et al**. Pseurotin a inhibits osteoclastogenesis and prevents ovariectomized-induced bone loss by suppressing reactive oxygen species. *Theranostics*. 2019;9(6):1634–1650.

46. **Ma Q**, **Liang M**, **Tang X**, **Luo F**, **Dou C**. Vitamin B5 inhibit RANKL induced osteoclastogenesis and ovariectomy induced osteoporosis by scavenging ROS generation. *Am J Transl Res*. 2019;11(8):5008–5018.

47. **Xie X**, **Liu M**, **Meng Q**. Angelica polysaccharide promotes proliferation and osteoblast differentiation of mesenchymal stem cells by regulation of long non-coding RNA H19: An animal study. *Bone Joint Res*. 2019;8(7):323–332.

48. **Deng S**, **Zhou JL**, **Fang HS**, **Nie ZG**, **Chen S**, **Peng H**. Sesamin protects the femoral head from osteonecrosis by inhibiting ROS-induced osteoblast apoptosis in rat model. *Front Physiol*. 2018;9:1787.

49. **Zhang S**, **Liu Y**, **Liang Q**. Low-dose dexamethasone affects osteoblast viability by inducing autophagy via intracellular ROS. *Mol Med Rep*. 2018;17(3):4307–4316.

50. **Cheng Y-Z**, **Yang S-L**, **Wang J-Y**, **et al**. Irbesartan attenuates advanced glycation end products-mediated damage in diabetes-associated osteoporosis through the AGEs/RAGE pathway. *Life Sci*. 2018;205:184–192.

51. **Xing LZ**, **Ni HJ**, **Wang YL**. Quercitrin attenuates osteoporosis in ovariectomized rats by regulating mitogen-activated protein kinase (MAPK) signaling pathways. *Biomed Pharmacother*. 2017;89:1136–1141.

52. **Wang N**, **Xu P**, **Wang X**, **et al**. Timosaponin AIII attenuates inflammatory injury in AGEs-induced osteoblast and alloxan-induced diabetic osteoporosis zebrafish by modulating the RAGE/MAPK signaling pathways. *Phytomedicine*. 2020;75:153247.

53. **Park M**, **Choi HK**, **An JH**. Taurine Activates BMP-2/Wnt3a-Mediated Osteoblast Differentiation and Mineralization via Akt and MAPK Signaling. *Iran J Public Health*. 2019;48(11):1960–1970.

54. **Li XJ**, **Zhu Z**, **Han SL**, **Zhang ZL**. Bergapten exerts inhibitory effects on diabetes-related osteoporosis via the regulation of the PI3K/AKT, JNK/MAPK and NF-κB signaling pathways in osteoprotegerin knockout mice. *Int J Mol Med*. 2016;38(6):1661–1672.

55. **Zhu W**, **Yin Z**, **Zhang Q**, **et al**. Proanthocyanidins inhibit osteoclast formation and function by inhibiting the NF-κB and JNK signaling pathways during osteoporosis treatment. *Biochem Biophys Res Commun*. 2019;509(1):294–300.

56. **Hou T**, **Zhang L**, **Yang X**. Ferulic acid, a natural polyphenol, protects against osteoporosis by activating SIRT1 and NF-κB in neonatal rats with glucocorticoid-induced osteoporosis. *Biomed Pharmacother*. 2019;120:109205.

57. **Kim B**, **Lee KY**, **Park B**. Icariin abrogates osteoclast formation through the regulation of the RANKL-mediated TRAF6/NF-κB/ERK signaling pathway in Raw264.7 cells. *Phytomedicine*. 2018;51:181–190.

58. **Li C-H**, **Xu L-L**, **Jian L-L**, **et al**. Stattic inhibits RANKL-mediated osteoclastogenesis by suppressing activation of STAT3 and NF-κB pathways. *Int Immunopharmacol*. 2018;58:136–144.

59. **Pengjam Y**, **Madhyastha H**, **Madhyastha R**, **Yamaguchi Y**, **Nakajima Y**, **Maruyama M**. NF-κB pathway inhibition by anthrocyclic glycoside aloin is key event in preventing osteoclastogenesis in RAW264.7 cells. *Phytomedicine*. 2016;23(4):417–428.

60. **Yang M**, **Xie J**, **Lei X**, **et al**. Tubeimoside I suppresses diabetes-induced bone loss in rats, osteoclast formation, and RANKL-induced nuclear factor-κB pathway. *Int Immunopharmacol*. 2020;80:106202.

61. **Noguchi T**, **Ebina K**, **Hirao M**, **et al**. Apolipoprotein E plays crucial roles in maintaining bone mass by promoting osteoblast differentiation via ERK1/2 pathway and by suppressing osteoclast differentiation via c-Fos, NFATc1, and NF-κB pathway. *Biochem Biophys Res Commun*. 2018;503(2):644–650.

Author information:
- Y. D. Liu, PhD, Surgeon, Department of Spine Surgery, The First Hospital of Jilin University, Changchun, China.
- J. F. Liu, MS, Surgeon
- B. Liu, PhD, Surgeon
  Department of Hand Surgery, The First Hospital of Jilin University, Changchun, China.

Author contributions:
- Y. D. Liu: Conceptualization, Data curation, Formal analysis, Writing – original draft.
- J. F. Liu: Data curation, Formal analysis.
- B. Liu: Conceptualization, Data curation, Formal analysis, Writing – review & editing.